LUND UNIVERSITY

FACULTY OF SCIENCE

In situ X-ray diffraction studies of vertically aligned $CsPbBr_3$ nanowire arrays

Jesper Larsson

Thesis submitted for the degree of Bachelor of Science
Project Duration: 2 months

Supervised by Jesper Wallentin

Department of Physics
Division of Synchrotron Radiation Research
June 2022

Abstract

The past decade has seen a great interest in the development of metal halide perovskite materials for use in photo-optical devices, due to the excellent photo-optical properties of these materials. The primary limitation to industrial adoption, and the subject of much research, is the susceptibility of these materials to degradation from exposure to various factors such as air, heat and moisture. Growing confined, vertical nanowire arrays of $CsPbBr_3$, a metal halide perovskite, has proven very effective in increasing resistivity to such degradation. In this project a method for *in situ* studies of such arrays of 170 nm diameter wires using X-ray diffraction is detailed. Measurements were also carried out on complete samples for comparison with the *in situ* sample. The crystal growth of the nanowires was found to be relatively quick process, and the crystal structure exhibited some preferential alignment early into the growth, although not to the extent observed in the complete samples. The crystal phase of the *in situ*-samples was the same as that of the complete sample, and corresponds well to calculated powder diffraction patterns of the orthorhombic *Pnmb* phase. The time resolution and data quality was limited by the in-house X-ray source, but the use of a more powerful source of X-ray radiation would allow for more detailed analyses of the phenomena studied as part of this project.

Abbreviations

- MHP - metal halide perovskite
- NW - nanowire
- DMSO - dimethyl sulfoxide
- AAO - anodised aluminium oxide
- SEM - scanning electron microscope
- PL - photo-luminescence
- XRD - X-ray diffraction

Contents

Acknowledgements

I would like to thank my supervisor, Dr. Jesper Wallentin of the Division of Synchrotron Radiation Research, for the indispensable guidance and assistance provided over the course of this project. I would also like to thank Dr. Johan Gustafson and Dr. Zhaojun Zhang, also of the Division of Synchrotron Radiation Research, for providing access to and instruction in the operation of the laboratory equipment used, and for the instruction and assistance in the growth of the $CsPbBr_3$ nanowire arrays respectively, as well as for valuable guidance and advice given.

1 Introduction

The last decade has seen a surge in the development of metal halide perovskite (MHP) materials, propelled largely by the promising photo-optical properties exhibited by them, making these materials suitable candidates for a wide variety of practical applications, ranging from photo-voltaic cells to laser devices. [1] Their photo-optical properties include a low density of midgap trap states, low nonradiative recombination rate, a high absorption coefficient, long carrier lifetime and highly efficient photo-luminescence. [2] An obstacle to reliable practical applications and thus wider industrial adoption, however, is their weakness to degradation as a result of exposure to moisture (and other polar solvents), light, heat and oxygen, leading to unwanted phase transitions. This susceptibility is owed to the soft ionic nature of such all-inorganic perovskites. [3]

In order to combat this issue, lead-halide perovskites have been grown in vertically confined arrays, producing micrometer-long nanowires (NW) which have been reported as having a much improved resistance to degradation from exposure to air, light and X-rays. This is owed to the shielding effects of the anodic aluminium oxide (AAO) membranes in which the wires are grown, and as a result the arrays showed neither any significant decrease in photo-luminescence nor any signs of degradation when studied using X-ray diffraction. There exists then an impetus for further studying these arrays and the crystallisation processes at play. [1], [4]

One of the most fundamental techniques for characterising crystal structures is that of X-ray diffraction (XRD), an invaluable method for structural determinations in fields ranging from solid state physics to structural biology. [5] XRD provides researchers with the ability to analyse a wide range of properties, including crystal size, shape, preferred orientations and internal strains or stresses of the crystal, as well as surface structures and the effects of varying temperatures on solids. [6] XRD is thus a clear candidate for studying these nanowire arrays and their growth.

The purpose of this project is thus to use XRD to perform *in situ* studies of $CsPbBr_3$ nanowire arrays. The goal is to utilise an in-house X-ray source to measure both the growth and the structure of $CsPbBr_3$ nanowire arrays, and to link these results to previous research and theory in order to provide insights into the growth process.

2 Theory

2.1 Crystal Structure, and Miller indices

A crystalline material is a solid material in which atoms are ordered in periodic, repeating patterns (in three dimensions). Mathematically we can describe crystals as lattices, where the locations of atoms make up the corresponding lattice points. These lattices are then divided into unit cells, constructed from the spatial distances (a, b and c) and the angles (α, β, γ) between the lattice points. A unit cell is then the smallest repeating unit which may be constructed out of these parameters for a given structure.

Drawing a coordinate system using these parameters above, and placing the origin in a corner of the unit cell, allows for the definition of vectors from the origin to intersecting points. Using the reciprocal points of these vectors as the parameters (h, k, l) we arrive at the convention of Miller indices, used to denote crystal planes in the lattice. [7]

2.1.1 Bravais lattice and the reciprocal lattice

The Bravais lattice is a mathematical object which may be used to represent a crystal structure using the parameters of the unit cell as described above, with the vectors $\boldsymbol{a_1}$, $\boldsymbol{a_2}$ and $\boldsymbol{a_3}$ pointing from the origin to the nearest lattice points. The Bravais lattice $\boldsymbol{R}$ is then defined as

$$\boldsymbol{R} = m\boldsymbol{a_1} + n\boldsymbol{a_2} + o\boldsymbol{a_3} \tag{1}$$

where m n and o are integers. The reciprocal lattice $\boldsymbol{G}$ for a given Bravais lattice $\boldsymbol{R}$ is then defined by the equation

$$\boldsymbol{G} \cdot \boldsymbol{R} = 2\pi l \tag{2}$$

where l is an integer. $\boldsymbol{G}$ may then be written as the sum of the three terms

$$\boldsymbol{G} = m'\boldsymbol{b_1} + n'\boldsymbol{b_2} + o'\boldsymbol{b_3} \tag{3}$$

where the vectors $\boldsymbol{b_1}$, $\boldsymbol{b_2}$ and $\boldsymbol{b_3}$ can be defined explicitly as [5]:

$$\boldsymbol{b_1} = 2\pi\frac{\boldsymbol{a_2} \times \boldsymbol{a_3}}{\boldsymbol{a_1} \cdot (\boldsymbol{a_2} \times \boldsymbol{a_3})}, \quad \boldsymbol{b_2} = 2\pi\frac{\boldsymbol{a_3} \times \boldsymbol{a_1}}{\boldsymbol{a_1} \cdot (\boldsymbol{a_2} \times \boldsymbol{a_3})}, \quad \boldsymbol{b_3} = 2\pi\frac{\boldsymbol{a_1} \times \boldsymbol{a_2}}{\boldsymbol{a_1} \cdot (\boldsymbol{a_2} \times \boldsymbol{a_3})}. \tag{4}$$

2.1.2 Cubic and orthorhombic crystal structure

Two simple cases of unit cells which may be described by a Bravais lattice is those of the cubic and orthorhombic crystal structures. In the former, we have equal lattice distances in all three directions ($a = b = c$) and only right angles between them ($\alpha = \beta = \gamma = 90°$). In the orthorhombic structure the same condition is applied to the angles as in cubic structures, but there are no equal spatial distances ($a \neq b \neq c$). [7]

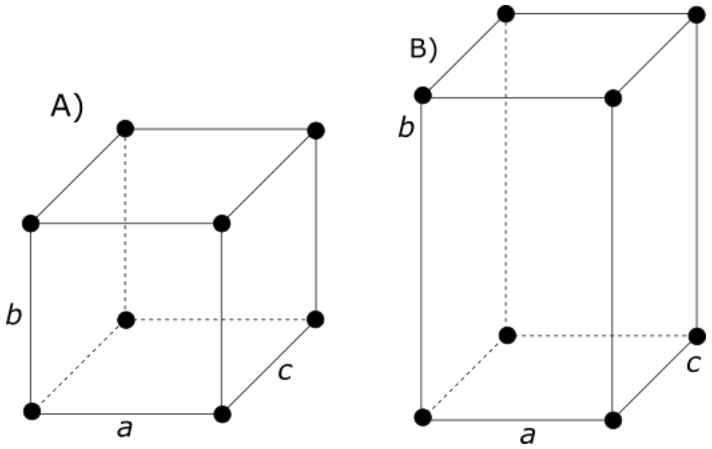

Figure 1: A) Typical cubic crystal structure B) Typical orthorhombic crystal structure

2.2 Crystal Growth and Nucleation Theory

While a description of crystal structures alone may suffice for studies limited to studying materials as they are, studying the growth of crystals requires some background information on how crystals are formed and grown. This occurs in two primary stages, nucleation, where the first crystal structures arise, and crystal growth, which is the stage in which these crystal nuclei begin to grow and form the larger crystal structure.

A condition for crystal nucleation and growth is supersaturation. A supersaturated solution is one in which the concentration of the solute is greater than the saturation (i.e. the equilibrium concentration), and is the fundamental driving force of crystallisation. Supersaturated solutions are metastable however, and will not necessarily begin to crystallise spontaneously, although this metastability decreases as the supersatuturation increases. In a supersaturated solution molecules begin to associate and form aggregates, unstable clusters of concentration fluctuations which dissolve by themselves. If the size of such a cluster reaches a critical size, however, it will not dissolving but instead begin to grow, causing nucleation to occur. This critical size is dependent on the degree of supersaturation, and decreases as supersaturation increases. As such, supersaturation becomes increasingly unstable, and the region between the beginning of supersaturation, and the point at which it becomes too unstable is known as the metastable zone, which is where all crystallisation operations occur. [8] For increasing supersaturation, nucleation theory predicts an exponential increase in nucleation rate with increasing supersaturation. [7]

The nucleation is as stated the first of what is often considered to be the two stages of crystallisation, the second being the aforementioned crystal growth. Considering the growth of a specific crystal face it becomes possible to understand why crystals grow layer by layer. A molecule dissolved in the supersaturated solution must be absorbed somewhere on the crystal structure, and the most energetically favourable positions are the ones which offer the most neighbouring molecules to connect to. In the case illustrated in fig.2 the most favourable sites are thus, in order, III, II and I. [7]

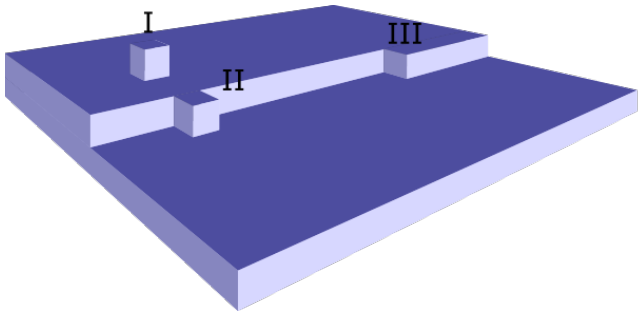

Figure 2: Possible sites for molecule absorption during crystal growth.

2.2.1 Solution Evaporation Growth

One technique for growing crystals is solution evaporation growth, wherein supersaturation is achieved via the evaporation of the solvent in a solution containing the crystal precursor. This allows for the control of the growth rate through the evaporation rate, and for maintaining the supersaturation necessary for crystal growth. It also ensures that the solution will always contain a reserve of precursor substances during evaporation. The downsides to this technique includes the concentration of impurities increasing as the solvent volume decreases, as well as increasing supersaturation during constant evaporation causing spurious nucleation, particularly in the miniscus or minsici of the solvent body. [9]

2.3 Perovskites

Perovskite materials make up a class of materials with the general formula ABX_3 which are ordered in the perovskite structure. The term perovskite as it refers to crystalline materials with this structure should not be confused with their namesake which is the calcium titanium oxide mineral of the same name, although this mineral is ordered in the same structure. The centre of the body is occupied by the A cation, which is surrounded by BX_6 octahedra, where the B cations occupy the centres of the octahedra (see fig.3). [10] In this description the location of the A cation is treated as the origin, with its location being the 1b sites with coordinates (0,0,0), B cations at 1a sites ($\frac{1}{2}$, $\frac{1}{2}$, $\frac{1}{2}$) and X at the 3c sites ($\frac{1}{2}$, $\frac{1}{2}$, 0); ($\frac{1}{2}$, 0, $\frac{1}{2}$); (0, $\frac{1}{2}$, $\frac{1}{2}$). The cations may also be displaced, and can as a result to give rise to e.g. cubic, tetragonal and orthorombic structures (phases). [11]

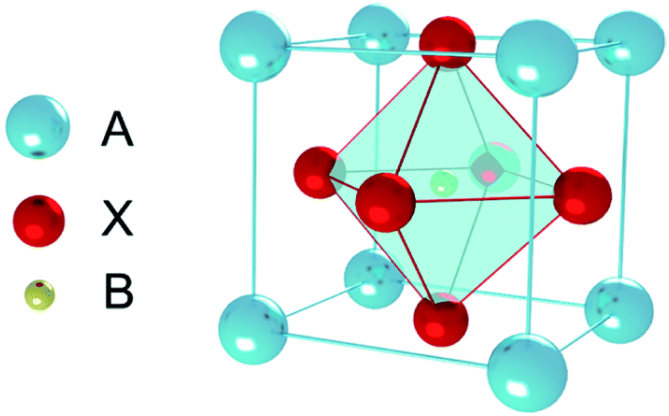

Figure 3: The typical ABX_3 structure. Courtesy of Chen et al. (2018) [12]

2.3.1 Metal Halide Perovskites

One of the most prominent recent developments in perovskite materials has been the development of metal halide perovskites (MHPs). In these materials the A cation is a monovalent cation, for example formamidinium (FA^+), methylammonium (MA^+) or caesium (Cs^+), while the B cation is a divalent metal such as lead (Pb^{2+}) or tin (Sn^{2+}). The X site is occupied by a halide such as bromide (Br^-) or iodide (I^-). [13]

In contrast with the currently predominant inorganic optoelectronic devices, which require complex and resource intensive manufacturing methods, MHPs can be manufactured using low-cost methods such as solution processing. [13] Furthermore MHP materials exhibit favourable properties for applications in optoelectronic devices, such as a low trap-state density [14] and associated long carrier diffusion lengths, making them highly suitable for use in photovoltaic cells. [15], [16] High photo-luminescence-efficiency [2] as well as tunable band-gaps contributes further to their suitability for use in devices. [1] They also benefit from an intrinsic tolerance to defects, as these are typically either very shallow, or located within the valence/conduction bands. [17]

The soft ionic nature of such inorganic perovskites are however a cause for significant instabilities, leading to degradation as a result of exposure to air, light, heat and moisture. [3] Stability is improved somewhat by the avoidance of methylammonium as a cation, owing to the intrinsic instability of MA-based hybrid halide perovskites. Inorganic halide perovskites, using for example caesium as the A cation, are instead more stable. These also lack organic hygroscopic cations, and as such degradation through hydration becomes less frequent. Nevertheless they still suffer degradation through decomposition, oxidation and polymorphic transition. [17]

2.3.2 Vertically Aligned $CsPbBr_3$ nanowire arrays

One method of significantly improving the resistance of caesium-lead halide perovskites against degradation has been the growth of vertically aligned $CsPbBr_3$ nanowire (NW) arrays. In this instance 50 µl of a precursor solution containing CsBr, $PbBr_2$ and dimethyl

sulfoxide (DMSO) was applied to a 100 μm thick anodised aluminium oxide (AAO) plate, containing nm-scale pores. The solution was then spin-coated before being placed on a hotplate set to 70°C.

Using this method the pores are filled completely with the precursor solution through spin coating, after which the nanowires are grown using solution evaporation, and exhibit single crystal growth as indicated by the faceted top of the wires when studied under a scanning electron microscope (SEM). The length of the wires was determined to be tunable through varying the amount of precursor solution applied to the AAO-plate. [1] The crystal structure of the $CsPbBr_3$ material could also be controlled via choosing AAO-plates with different pore sizes, with the $CsPbBr_3$ adopting a cubic structure when grown in pores with a diameter of 20nm or smaller. For greater pore diameters (>40 nm) the orthorhombic structure was instead observed. X-ray diffraction measurements showing a single (002)-peak in the former case and a split (004)/(220)-peak in the second was used to discriminate between the two.

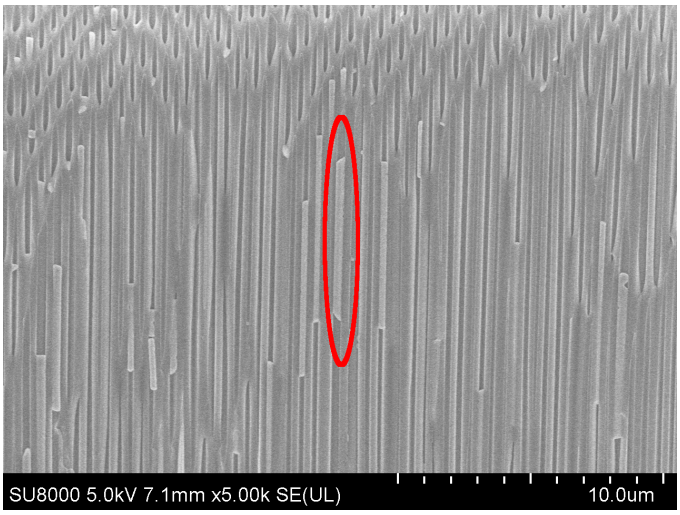

Figure 4: SEM image of a $CsPbBr_3$ NW array with 170 nm diameter pores. Image courtesy of Dr. Zhaojun Zhang

Comparative measurements between freshly grown samples and samples stored in air for 4 months showed no significant decrease in PL intensity. Repeated XRD measurements showed no diffraction peaks corresponding to degradation products. Furthermore tests on the resistivity of the NW arrays to X-ray radiation showed no decrease in scintillation following irradiation, and an increase in scintillation was noted instead. The improved stability of these NW arrays as opposed to e.g. thin MHP-films is ascribed to the encapsulation effect of the AAO. [1]

In later developments these NW arrays have been grown using a modified method, wherein a precursor solution consisting of 0.4M $CsPbBr_3$ dissolved in DMSO, yielding pure-phase $CsPbBr_3$. A 50 μm thick AAO membrane (purchased from Topmembranes Technology Ltd., with diameters of 25mm and 13mm), with the nanopores open at both ends, is then placed on top of the solution, allowing capillary forces to fill the pores with the precursor solution. After being left for one minute to ensure the pores being filled the slides were moved to a hotplate set to 70°. [4]

2.4 X-ray Scattering and Diffraction

2.4.1 Bragg Theory

X-ray diffraction is one of the most important tools for determining crystal structures. Since X-rays interact weakly with matter we may use the kinematic approximation, i.e. that X-rays are restricted to either single scattering or not interacting at all. Furthermore the X-ray source is assumed to be placed far away from the sample to be studied, such that the X-rays can be considered plane waves. This is then the basis for the Bragg theory of diffraction, as first formulated in 1912.

In this treatment we consider plane waves of X-rays incident on crystal planes with some incidence angle $90° - \theta$. In this case there will be constructive interference given that the difference in distance traversed by X-rays reflected from one layer compared with those reflected from the next corresponds to an integer multiple of the X-rays wavelength λ. This gives rise to the Bragg condition, or Bragg's Law, for X-ray scattering

$$n\lambda = 2d \sin\theta \tag{5}$$

where d is the spacing between the crystal planes which give rise to the diffraction. By the geometry of this problem, if Bragg's law holds for one pair of layers, it must hold for all layers with equal spacing, each contributing to the constructive interference pattern. This then allows for the identification of different phases, provided that the spacing between lattice points is known. This is an admittedly simplistic treatment, yet not necessarily an inaccurate one, as Bragg's law is a specific case of more general X-ray diffraction theory.

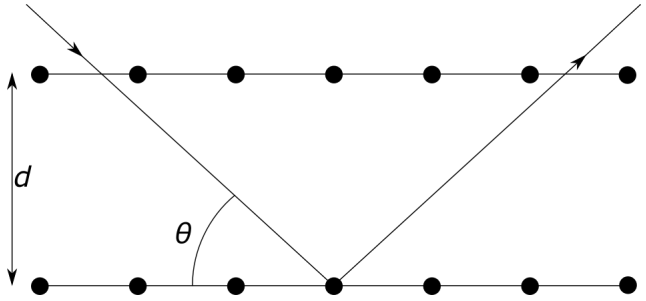

Figure 5: The geometry of Bragg diffraction.

2.4.2 General Diffraction Theory

In this more general approach we consider the physical mechanism behind the scattering of the X-rays, namely the induction of oscillations in the electrons orbiting an atom, oscillations which will inherit the frequency of the incoming X-ray radiation, and which will lead to the emission of X-rays, giving rise to an interference pattern. In this case the scattering is not simply photons impinging off on atoms, but is due to the electrons surrounding them, and as such the scattered intensity will be dependent on the electron density $\rho(\boldsymbol{r})$ in the material. However, since most electrons are (relatively) located very

close to the atoms one can still relate this to the lattice points based on the positions of the atoms.

Assuming both the X-ray source and the detector is located sufficiently far away to allow us to consider the incoming and scattered EM-waves to be plane waves, and for an incoming wavevector $\boldsymbol{k}$ and scattered wavevector $\boldsymbol{k'}$ (with $\boldsymbol{K} = \boldsymbol{k'} - \boldsymbol{k}$), the intensity I observed will be proportional to $\rho(\boldsymbol{r})$ over the crystal volume V via the expression

$$I(\boldsymbol{K})\alpha \left| \int_V \rho(\boldsymbol{r}) \exp^{-i\boldsymbol{K}\cdot\boldsymbol{r}} dV \right|^2 . \tag{6}$$

The equation (2) can then be reformulated by replacing the electron density with a Fourier series over the reciprocal lattice, resulting in a lattice-periodic electron density $\rho(\boldsymbol{r}) = \sum_{\boldsymbol{G}} \rho_{\boldsymbol{G}} \exp^{-i\boldsymbol{G}\cdot\boldsymbol{r}}$ yielding the expression

$$I(\boldsymbol{K})\alpha \left| \sum_{\boldsymbol{G}} \int_V \rho_{\boldsymbol{G}} \exp^{i(\boldsymbol{G}-\boldsymbol{K})\cdot\boldsymbol{r}} dV \right|^2 . \tag{7}$$

For large crystals the crests and troughs of the wave will cancel and the integrals will be very small, with the exception of the cases when the Laue condition

$$\boldsymbol{K} = \boldsymbol{k'} - \boldsymbol{k} = \boldsymbol{G} \tag{8}$$

is fulfilled, which is then the condition for observing constructive interference from scattered X-rays.

Applying this to the case of Bragg diffraction it becomes clear that it. For a vector with three components the Laue condition can be viewed as three separate conditions, two of which are satisfied due to the geometry of Bragg diffraction. The condition is then

$$k_\perp - k'_\perp = 2k_\perp = 2\frac{2\pi}{\lambda}\sin\theta = G \perp \tag{9}$$

where $G_\perp$ is a vector of the reciprocal lattice, perpendicular to the crystal planes studied.[5]

2.4.3 Diffraction in the cubic and orthogonal $CsPbBr_3$ phases.

Of particular interest for the characterisation of $CsPbBr_3$ is, as mentioned, the diffraction peak of the (0,0,2) crystal plane in the *Pm-3m* cubic phase, and the split peaks stemming from diffraction in the (0,0,4)/(2,2,0) planes in the orthorhombic *Pnmb* phase. [1]

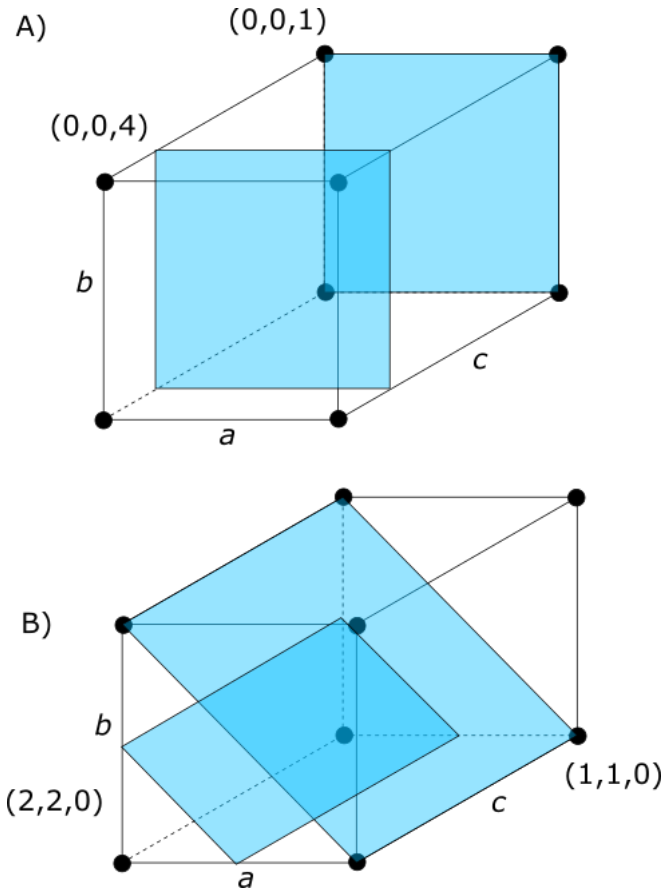

Figure 6: A): The (0,0,4) and (0,0,1) planes of a cubic structure. B): The (1,1,0) and (2,2,0) planes of an orthorhombic crystal structure.

The unit cell of the cubic *Pm-3m* has the dimensions $a = b = c = 5.871$ Å, and the orthogonal *Pnmb* unit cell has the dimensions $a = 8.207$ Å, $b = 8.255$ Å and $c = 11.759$ Å. [1]

2.4.4 GIWAXS

A method which has proven suitable for *in situ* studies of perovskite films is Grazing-Incidence Wide-Angle X-ray Scattering (GIWAXS). GIWAXS as a technique differs from other types of scattering primarily when it comes to the geometry of the scattering. In GIWAXS the sample is illuminated by a beam of X-ray light with a very small (grazing) incidence angle. One significant advantage of this technique is that it allows for control over the probing depth, as the energy of the X-ray beam in use determines the amount of material penetrated by the beam. Another feature, albeit one which is not exclusive to GIWAXS, is the use of 2D detectors, allowing for the characterisation of highly ordered structures thanks to the ability to observe in both the in-plane and out-of-plane directions. [18]

3 Method

3.0.1 Equipment, Laboratory set up and calibration

The experimental setup consists of a Pilatus CdTe 300k X-ray detector, situated opposite of a 17.45kev Genix 3D X-ray source. Between these two pieces of equipment is a stand for mounting samples and other equpment, fitted with remotely controlled servo motors allowing for movement in seven axes. Mounted on the stand is a hotplate, which is used to drive the $CsPbBr_3$ NW growth.

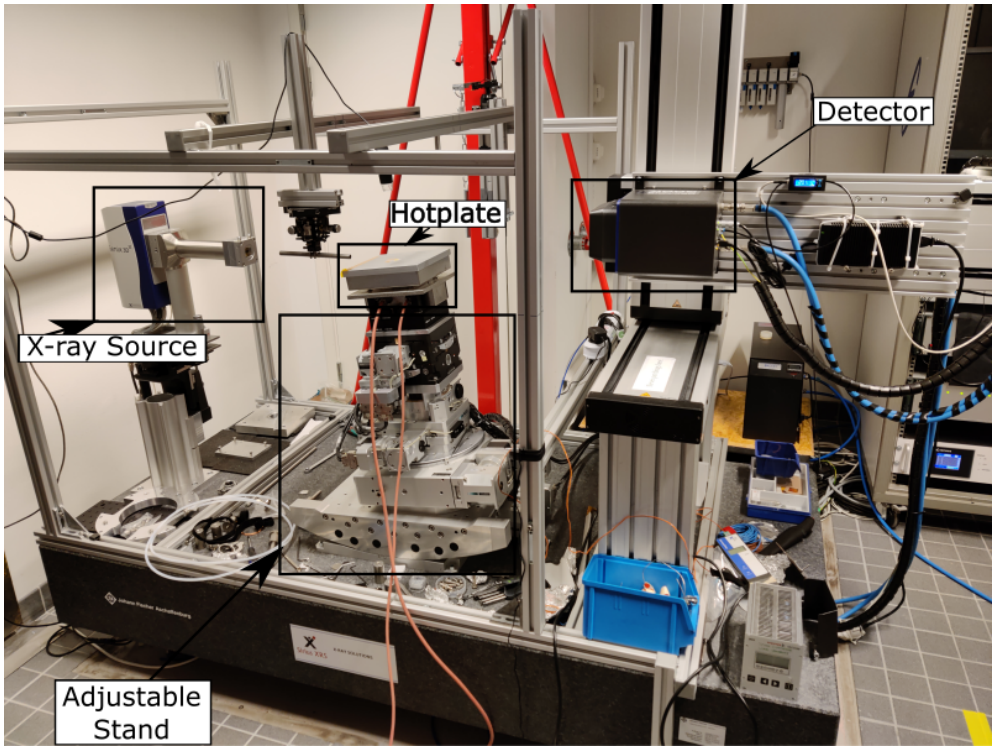

Figure 7: Lab setup showing the equipment used for the purpose of this project.

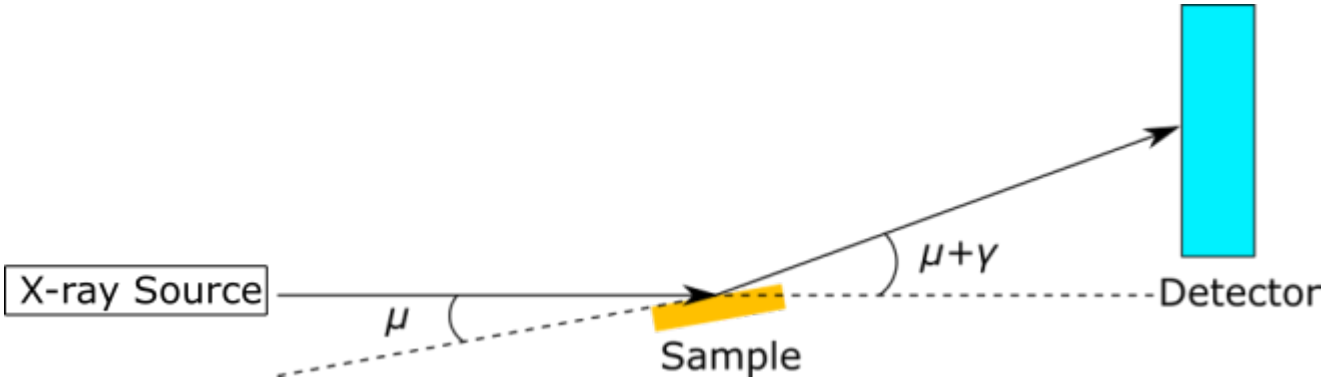

Figure 8: Geometry of the laboratory set-up.

The angles μ between the sample and γ between the sample and detector are each controlled by a separate servo, and are used to control the incidence angle between the beam and the sample and the position of the detector.

In order to relate the pixels of the detectors to real-world positions, in terms of the angle 2θ and the azimuthal angles along diffraction rings a calibration using lanthanum hexaboride (LaB_6) as a calibrant is performed by performing a 1 minute XRD-measurement on a sample of LaB_6. This measurement is then used in conjunction with the pyFAI (Fast Azimuthal Integration) python library, which includes a program which uses the diffraction pattern of a known calibrant to relate the detector pixels to real-world positions.

Theoretical values for the diffraction pattern of the $CsPbBr_3$ *Pnmb* phase was calculated using the Cambridge Crystallographic Data Centre's Mercury software (version 4.1.0) for an X-ray energy of 17.45 keV. [20]

3.1 Experimental Process

3.1.1 Measurements on fully grown samples

A complete sample of $CsPbBr_3$-nanowires were initially studied using the experimental setup described above. In this case a series of measurements were performed with 5 minute exposure times for a range of incidence angles μ ranging from $0 - 11°$ and γ ranging from $8 - (-3)°$, with a measurement performed every $0.1°$ The resulting detector images were then analysed using the pyFAI (Fast Azimuthal Integration) python library [21] in both one dimension, integrating azimuthally for specific 2θ values, and in two dimension, taking into account both the 2θ-values and azimuthal position of diffraction peaks. A followup measurement was taken at $\mu = 7°$ and $\gamma = 1°$.

3.1.2 In-Situ Growth Measurements

$CsPbBr_3$ NW-arrays with a pore diameter of (170nm) are grown via the method detailed above and in [4]. 10 µl of the precursor solution, consisting of 0.3M $CsPbBr_3$ in solution using DMSO as a solvent, is applied to a thin glass substrate, located atop the hotplate heated up to the growth temperature of 70°C. Following this a piece of AAO-plate is placed upon the drop of precursor solution, and once this is done the room in which the experiment is to take place in is vacated, and the shutter of the X-ray source is opened and the measurements begin. For this experiment the angles $\mu = 7°$ and $\gamma = 1°$ were set and maintained throughout the duration of the experiment. A camera was also used to film the growth experiments.

The measurement consisted of an initial series of 720 scans (each with an exposure time of 5 seconds) starting approximately 30 seconds following the application of the precursor solution to the substrate, and then followed by a series of one minute long scans over the course of three hours. These images were used alongside a calibration measurement taken immediately before the specific in-situ measurement analysed.

Data analysis were performed using pyFAI, which was used to produce both one-dimensional (looking only at 2θ-values) and two-dimensional (looking at both 2θ-values and azimuhtal angles) analyses of the data, which was subsequently plotted.

4 Results

4.1 Measurements on complete NW Samples

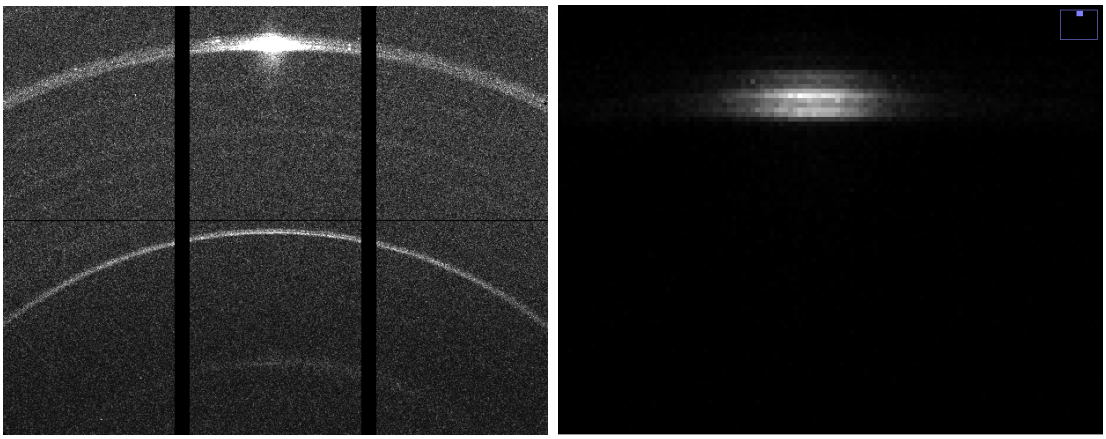

Figure 9: Left: Detector image showing the diffraction pattern of the finished sample, with diffraction rings with lower 2θ-values towards the bottom of the image. Right: Zoomed in view of the detector image of the (0,0,4)/(2,2,0) split peak.

Fig.9 shows the detector image from initial XRD measurement performed on a complete $CsPbBr_3$ NW sample with a 170 nm pore diameter, and clearly shows diffraction rings, with the rings being ordered from the bottom to the top by their corresponding 2θ-value, with increasing values towards to top of the image. Fig.9 also shows a high degree of azimuthal alignment with some 65.0% of the intensity being concentrated in the arc spanning the azimuthal angles $80° \leq \chi \geq 100°$ along the diffraction ring of the (0,0,4)/(2,2,0) planes (where 90° corresponds to the direction point directly up in fig.9). The measurements also show a split in the (0,0,4)/(2,2,0) peaks. This split was more visible when plotting the intensity as a function of the 2θ-value in fig.10.

As can be seen in fig.10, the measured diffraction pattern matches the calculated pattern for $CsPbBr_3$ powder obtained from the Mercury software, with both the major (1,1,2) and split (0,0,4)/(2,2,0) peaks, and the minor peaks at $2\theta = 12°$ and $2\theta = 13°$ mathing. The measurement also matches the results from XRD-measurements performed on similair NW arrays with pore diameters of 160 nm and 170 nm, as performed by Zhang et al. (2021,2022) in their papers. [1],[4]

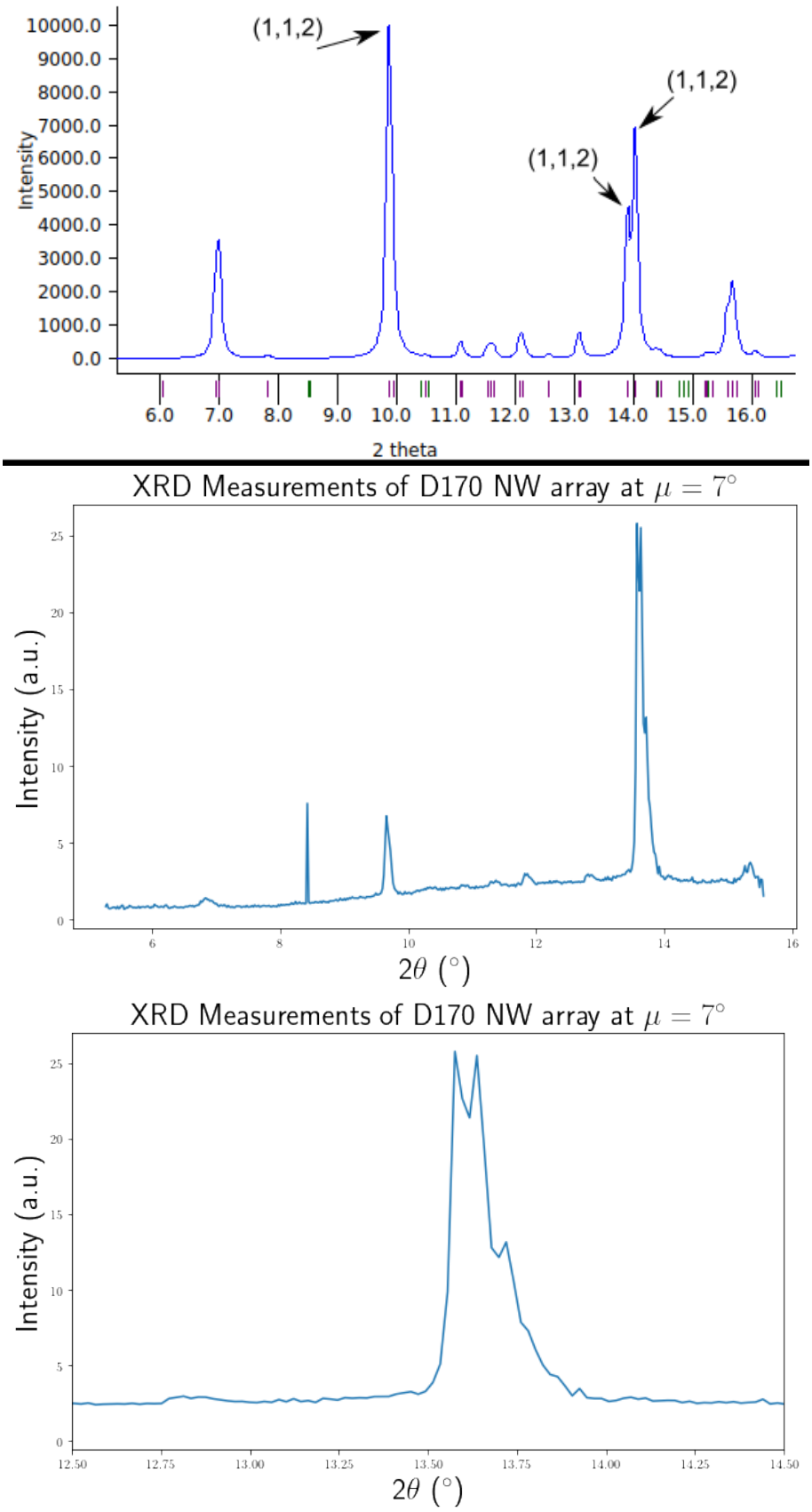

Figure 10: Top: Calculated diffraction pattern for the *Pnmb* phase of $CsPbBr_3$ powder. Middle: Diffraction pattern of the finished sample. Bottom: Zoomed in view of the (0,0,4)/(2,2,0) split peak (the left and middle peak respectively).

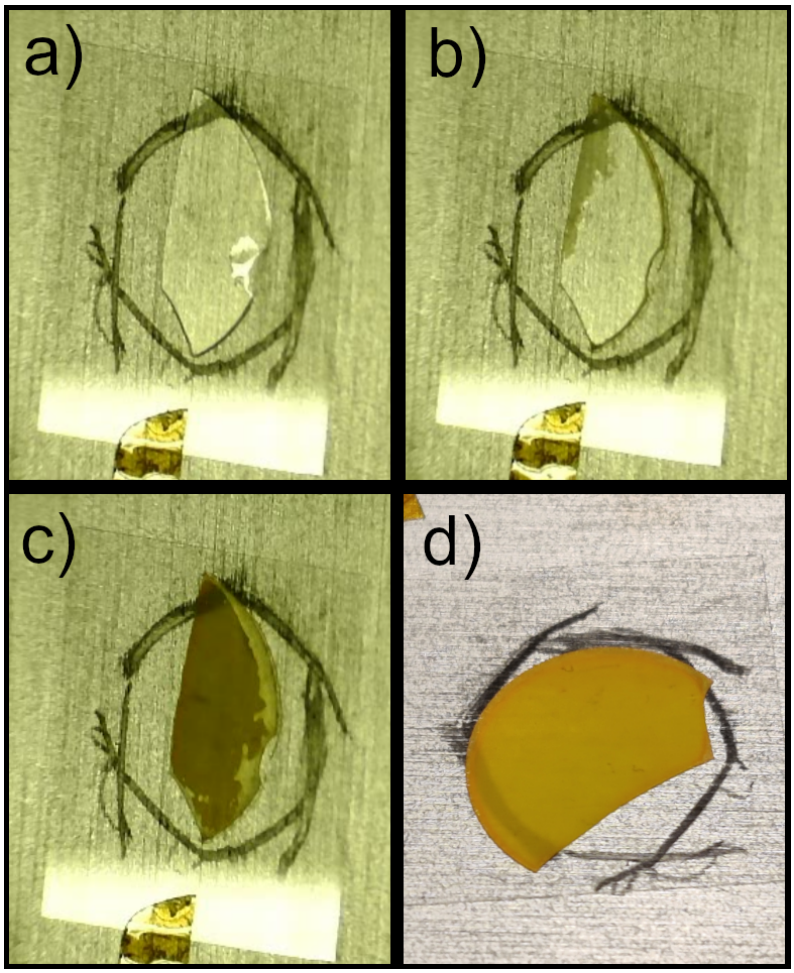

Figure 11: a) AAO plate immediately after having been placed on the precursor solution. b) Initial Growth beginning from the edges, 2 minutes and 25 seconds from the start of the growth experiment. c) The sample approximately 18 minutes after the start of the experiment. d) Another sample the night after a growth example

4.2 *In situ* Growth Measurements

4.2.1 Crystal Nucleation and Growth

Preceding the measurements of *in situ* growth, films were shot of growth experiments, producing the stills shown in fig.11. In this film the growth begins approximately 2 minutes and 25 seconds after the AAO membrane is placed atop the glass substrate, and lasts for roughly 1 minute and 15 seconds. The *in situ* measurements performed on the growing NW arrays show a rapid transition from the precursor stage to the saturated state, visualised as the sudden appearance of the diffraction rings at $2\theta = 9.7°$ and $2\theta = 13.8°$ in fig.12, emerging shortly after frame 15 of the measurement, corresponding to 1 minute and 15 seconds into the measurement.

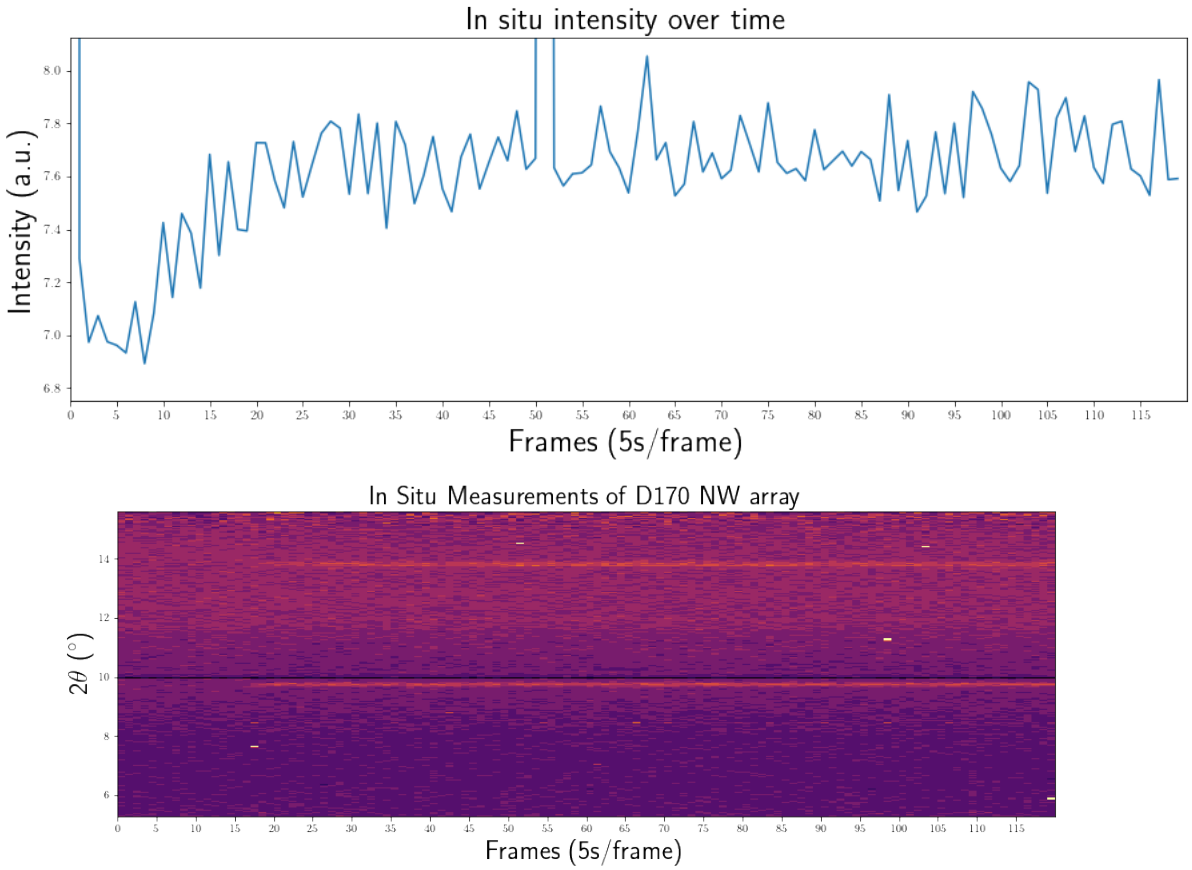

Figure 12: Top image: Intensity growth over time, showing the nucleation and crystal growth. Bottom image: Emergence of the observed diffraction peaks around frame 15.

This growth is shown in greater detail when looking at the growth in intensity in the 2θ-intervals $9.6 = 9.9°$ and 2θ-intervalls $9.6 = 9.9°$. From the top subfigure in fig.12 it's shown that intensity begins to increase after the tenth frame, approximately 80 seconds after the beginning of the XRD-measurement. This growth last until roughly frame 25, corresponding to 1.25 minutes of growth ending at 2 minutes and 5 seconds into the measurement. Snapshots of the growth of another sample is also shown in fig.11.

This results fits well with available knowledge on nucleation and crystal growth theory, as well as the solution evaporation technique for crystal growth. The 'dormant' period encompassing the first 1.5 minutes is then likely the period during which concentrations, beginning at below thermodynamical equilibrium, increase and enter the supersaturated zone. As it does so the nucleation rate increases exponentially, until nucleation begins to occur followed by plane-wise crystal growth, proceeding quite rapidly as more solution is evaporated away, maintaining supersaturation until no solvent remains and all crystallisation is complete. It also matches the description of crystallisation of thin films provided by Qin M, Chan P F, Lu X, (2021) [18]

4.2.2 Characterisation of *in situ* Nanowires

Characterising the freshly grown NW arrays is possible through analysing both the diffracted intensity as a function of the 2θ-value and the alignment of the structures as seen through the azimuthal distribution of the diffracted intensity. As visible from fig.13 the freshly grown sample exhibits the split (0,0,4)/(2,2,0)-diffraction peaks at $2\theta \approx 13.8°$, which are characteristic of the orthorhombic *Pnmb* $CsPbBr_3$ phase. The split itself corresponds well to the split visible in fig.10, and the split is also visible when studying the 2D nature of the diffraction visible in fig.15b. This split, as well as the noticeable azimuthal alignment of the diffraction peaks is also visible early on, and can be observed from the 24-36th frames and onwards, as can be seen in fig.14b. Compared to the complete sample however only 37.4% of the intensity is contained in the arc spanning the azimuthal angles $80° \leq \chi \geq 100°$ along the (0,0,4)/(2,2,0) diffraction ring.

It is notable that, while present, the vertical alignment is significantly less prominent than in the fully grown samples. The cause of this is unknown, but it could be speculated to emerge as a result of the modified growing method. In the method involving the spin-coating of AAO-plates with only one open end it was concluded that nanowires were the result of single crystal growth. In the case of the modified method used in this experiment it is not unthinkable that lack of a delay to allow capillary forces to fill the pores before placing the sample on the hotplate contribute to less uniform crystal growth. It is also not unthinkable that having both ends open allow for excessive nucleation in the minisci of the pores as supersaturation increases during the evaporation of the solvent.

The in situ measurement seems to be vulnerable to noise, likely due the relatively low power of the in-house X-ray source makes the measurements vulnerable to noise, e.g. from cosmic rays and Compton scattering of the X-ray beam against atoms in the air. This vulnerability is especially noticeable in the top figure of fig.12, with two large and otherwise inexplicable peaks in measured intensity.

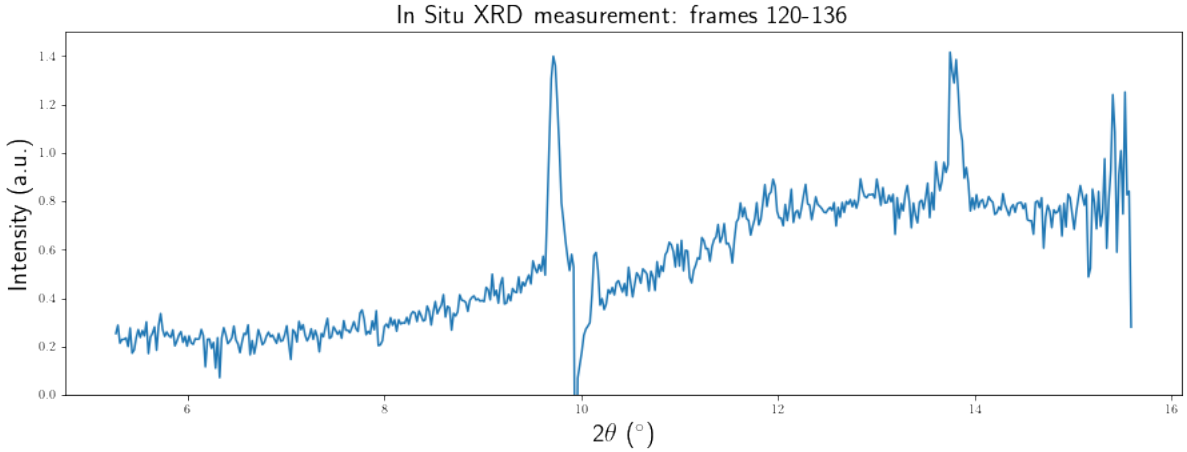

Figure 13: Diffraction pattern of the *in situ* sample, measured during frames 120-132

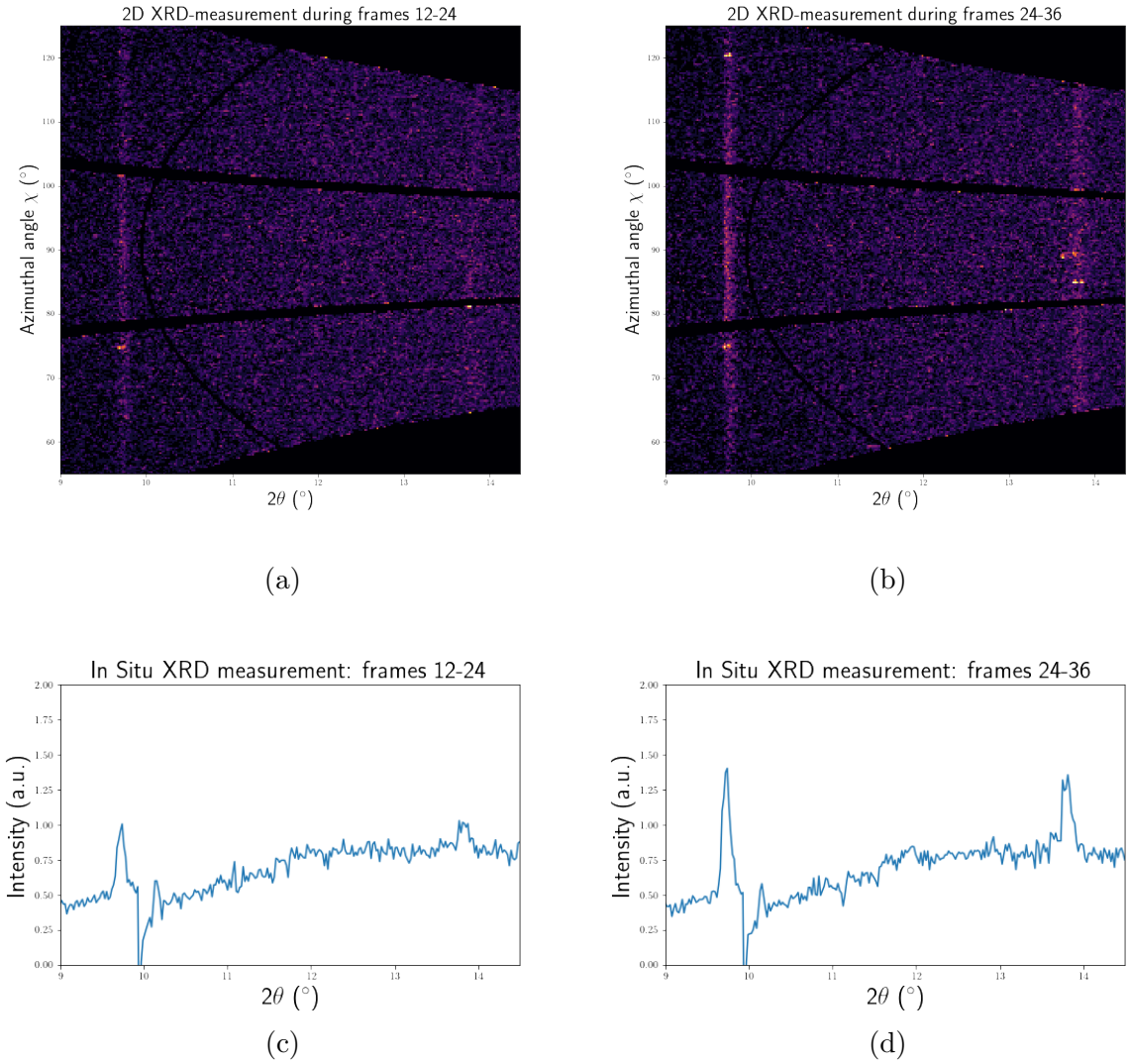

Figure 14: a/b) 2D XRD Measurements showing azimuthal orientation of diffraction patterns. c/d) XRD Diffraction peaks measured during the same time periods.

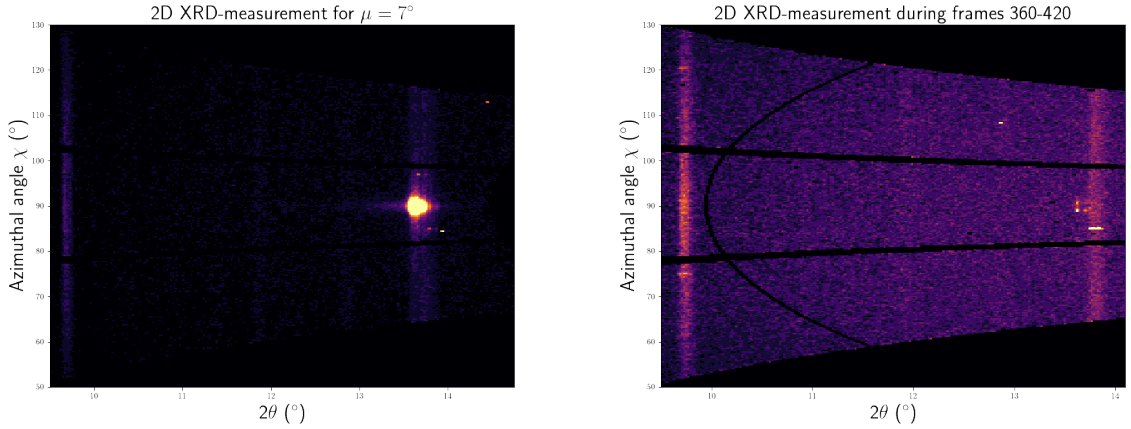

(a) (b)

Figure 15: 2D XRD Measurements showing azimuthal alignment of diffraction patterns in a) the complete sample, and b) the *in situ* sample.

5 Conclusions

The promising photo-optical properties of metal-halide perovskites, with $CsPbBr_3$ being one of these materials, make them promising candidates for use in a variety of important industrial applications, but their adoption is thus far hampered by an instability to degradation resulting from exposure to air, moisture heat and light. A method which significantly increases resistance to such degradation has been the growing of $CsPbBr_3$ nanowire arrays enclosed in AAO membranes, leading to much improved stability in air, and under exposure to light and X-rays.

X-ray diffraction using an in-house X-ray source was shown to be a functional method for analysing the crystal growth and structure of these NW arrays, although limited in resolution w.r.t. time and sensitive to light and noise, a limitation remediable through the use of more powerful X-ray sources such as a synchrotron. Despite this it was possible to identify that the wires grow relatively quickly, with crystal growth lasting only for about one and a half minute, matching both theoretical descriptions and precious research on lead-halide perovskite growth. The wires are also appear to adopt an orthorhombic crystal structure without undergoing phase-transitions. The wires grown *in situ* displayed were noticeably less oriented when compared to the older sample, and while the source of this discrepancy is not known with certainty, both the experimental method causing less uniform deposition of precursor solution in the pores, and the membranes used causing superfluous nucleation are plausible explanations.

6 Outlook

This project has arrived at a viable method for performing *in situ* analyses of perovskite nanowire arrays using an in-house X-ray source. This method can be used to study both the crystal growth in terms of its onset and duration, as well as structural properties such as preferential alignment in structures thanks to the the use of a 2D X-ray detector. The major limiting factor of this method however is the in-house X-ray source, which, although being a relatively accessible implement, does lead to sensitivity to noise originating from e.g. cosmic rays, as well as lower limits on the time resolution of the measurements. The use of more powerful X-ray sources, such as a synchrotron, could allow for more detailed studies, particularly of the fairly rapid nucleation and crystal growth process, shedding more light on the factors affecting these processes.

References

[1] Zhang Z, Suchan K, Li J, Hetherington C, Kiligaridis A, Unger E, et al. Vertically Aligned CsPbBr3 Nanowire Arrays with Template-Induced Crystal Phase Transition and Stability. *J. Phys. Chem. C* 2021 Feb 11; 125 (8), 4860-4868. Available from: https://doi.org/10.1021/acs.jpcc.0c11217

[2] Yang Z, Lu J F, ZhuGe M H, Cheng Y, Hu J F, Li F T, et al. Controllable Growth of Aligned Monocrystalline CsPbBr3 Microwire Arrays for Piezoelectric-Induced Dynamic Modulation of Single-Mode Lasing. *Adv. Mater.* 2019 Mar 25; 31(18), 1900647. Available from: https://doi-org.ludwig.lub.lu.se/10.1002/adma.201900647

[3] Zhang C, Chen J, Kong L, Wang L, Wang S, Chen W, et al. Core/Shell Metal Halide Perovskite Nanocrystals for Optoelectronic Applications. *Adv. Funct. Mater.* 2021 Mar 3; 31(19) 2100438 Available from: https://doi.org/10.1002/adfm.202100438

[4] Zhang Z, Dierks H, Lamers N, Sun C, Nováková K, Hetherington C, et al. Single-Crystalline Perovskite Nanowire Arrays for Stable X-ray Scintillators with Micrometer Spatial Resolution *Apl. Nano Mater.* 2022 Jan 28; 5 (1), 881-889, Available from: https://doi.org/10.1021/acsanm.1c03575

[5] Hofmann P, Solid State Physics - An introduction, 2nd edition, Weinheim, Wiley-VCH Verlag GmbH & Co, 2015, Pages 7-17

[6] Gonon M, Case Studies in the X-ray Diffraction of Ceramics In: Pomeroy M, Encyclopedia of Materials: Technical Ceramics and Glasses, Volume 1, Elsevier, c2021, Pages 560.-577

[7] Schwartz A M, Myerson A S, Crystals, crystal growth, and nucleation, In: Myerson A S, Handbook of Industrial Crystallization, 2nd Edition, Butterworth-Heinemann, c2002, Chapter 2, Available from: https://doi.org/10.1016/B978-075067012-8/50004-5

[8] Schwartz A M, Myerson A S, Solutions and solution properties, In: Myerson A S, Handbook of Industrial Crystallization, 2nd Edition, Butterworth-Heinemann, c2002, Chapter 1, Available from: https://doi.org/10.1016/B978-075067012-8/50003-3

[9] Pritula I, Sangwal K, Fundamentals of Crystal Growth from Solutions, In: Rudolph P, Handbook of Crystal Growth, 2nd Edition, Elsevier, c2015, Chapter 29, Available from: https://doi.org/10.1016/B978-0-444-63303-3.00029-8

[10] Rao C N R, Perovskites, In: Meyers R A, Encyclopedia of Physical Science and Technology, 3rd edition, Academic Press, c2003 [cited 2022 04 19], pages 707-714, Available from: https://doi.org/10.1016/B0-12-227410-5/00554-8

[11] Burns G, Glazer A M, Space Groups for Solid State Scientists, 3rd Edition, Academic Press, c2013 [cited 2022 04 19], Chapter 7: Space Group Applications, pages 213-217, Available from: https://doi.org/10.1016/B978-0-12-394400-9.00007-1.

[12] Figure: Chen Y, Zhang L, Zhang Y, Gao H, Yan H, Large-area perovskite solar cells – a review of recent progress and issues, *RSC Adv.*, 2018 Mar 14, 8, 10489-10508, Figure 3: ABX_3 perovskite structure. Available from: https://doi-org.ludwig.lub.lu.se/10.1039/C8RA00384J Licensed under CC BY 3.0 (https://creativecommons.org/licenses/by/3.0/legalcode)

[13] Wu S, Chen Z, Yip H-L, Jen A K-Y, The evolution and future of metal halide perovskite-based optoelectronic devices, *Matt.*, 2021 Dec 01; 4(12), 3814-3834. Available from: https://doi.org/10.1016/j.matt.2021.10.026

[14] Shi D, Adinolfi V, Comin R, Yuan M, Alarousu E, Buin A, et al. Low trap-state density and long carrier diffusion in organolead trihalide perovskite single crystals. *Science* 2015 Jan 30; 347(6221), 519-522. Available from: https://doi.org/10.1126/science.aaa2725

[15] Stranks S D, Eperon G E, Grancini G, Menelaou C, Alcocer M J P, Leijtens T, et al. Electron-Hole Diffusion Lengths Exceeding 1 Micrometer in an Organometal Trihalide Perovskite Absorber. *Science* 2013 Oct 18; 342(6156) 341-344 Available from: https://doi.org/10.1126/science.1243982

[16] Xing G, Mathews N, Sun S, Lim S S, Lam Y M, Grätzel M, et al. Long-Range Balanced Electron- and Hole-Transport Lengths in Organic-Inorganic $CH_3NH_3Pbl_3$ *Science* 2013 Oct 18; 342(6156) 344-347 Available from: https://doi.org/10.1126/science.1243167

[17] Zhou Y, Zhao Y, Chemical stability and instability of inorganic halide perovskites *Energy Environ. Sci.* 2019 Mar 7; 12, 1495-1511 Available from: https://doi-org.ludwig.lub.lu.se/10.1039/C8EE03559H

[18] Qin M, Chan P F, Lu X, A Systematic Review of Metal Halide Perovskite Crystallization and Film Formation Mechanism Unveiled by *In Situ* GIWAXS. *Adv. Mater.* 2021 Oct 04 33(51) 2105290. Available from: https://doi.org/10.1002/adma.202105290

[19] Xu Y, Chen Q, Zhang C, Wang R, Wu H,Zhang X, et al. Two-Photon-Pumped Perovskite Semiconductor Nanocrystal Lasers *J. Am. Chem. Soc.* 2016 Mar 3; 138(11) 3761–3768 Available from: http://dx.doi.org/10.1021/jacs.5b12662

[20] The Cambridge Crystallographic Data Centre, Mercury - Crystal Structure Visualisation, Exploration and Analysis Made Easy, [cited 2022 May 01], Available from: https://www.ccdc.cam.ac.uk/solutions/csd-core/components/mercury/

[21] Data analysis unit, European Synchrotron Radiation Facility, Grenoble, Fast Azimuthal Integration using Python, c2012-2022, [cited 2022 May 01] Available from: https://pyfai.readthedocs.io/en/master/

A Code used in data analysis

The following pieces of Python computer code were used, in the form of Jupyter Notebooks, to analyse and plot data obtained in the XRD measurements.

A.0.1 Finished Sample

```
import time
import shutil, os
from silx.resources import ExternalResources
import pyFAI, fabio
import glob

# clean-up files from previous run:
for result in ('integrated.edf', "integrated.dat"):
    if os.path.exists(result):
        os.unlink(result)

path = os.path.abspath("[path to data folder]")
files = glob.glob(path + '/*.dat')

import numpy as np
i = -1

data_list = []

for dfile in files:
    i += 1
    data = np.loadtxt(dfile, dtype=float)
    print("entry ", i, " read:")
    print(data)
    print(data.shape)
    data_list.append(data)

data_array = np.asarray(data_list)
print(data_array)
print(data_array.shape)

import matplotlib.pyplot as plt
from matplotlib.colors import BoundaryNorm
from matplotlib.ticker import MaxNLocator
import numpy as np
import matplotlib as mpl
from matplotlib.pyplot import subplots

plt.rcParams['text.usetex'] = True

Y = data_array[0, 0:, 1]
X = data_array[0, 0:, 0]
fig, ax = plt.subplots(figsize=(10,6))

ax.set_title(r"XRD Measurements of D170 NW array at $\mu=7^{\circ}$",
      fontsize = 24, color = 'k')
ax.set_xlabel(r"2$\theta$ ($^{\circ}$)",
```

```
      fontsize = 24, color = 'k')
ax.set_ylabel(r"Intensity (a.u.)",
      fontsize = 24, color = 'k')
plt.plot(X,Y)

Y = data_array[0, 0:, 1]
X = data_array[0, 0:, 0]
fig, ax = plt.subplots(figsize=(10,6))

ax.set_xlim(12.5,14.5)
ax.set_title(r"XRD Measurements of D170 NW array at $\mu=7^{\circ}$",
      fontsize = 24, color = 'k')
ax.set_xlabel(r"2$\theta$ ($^{\circ}$)",
      fontsize = 24, color = 'k')
ax.set_ylabel(r"Intensity (a.u.)",
      fontsize = 24, color = 'k')
plt.plot(X,Y)

all_images = glob.glob(path + '/*.tif')
ai = pyFAI.load("[path to calibration .poni file]")

cakedata_list = []
I_list = []
tth_list = []
chi_list = []

for one_image in all_images:
    fimg = fabio.open(one_image)
    dest = os.path.splitext(one_image)[0] + "_cake.edf"
    cake1 = ai.integrate2d_ng(fimg.data,
                    500, 360,
                    unit="2th_deg",
                    filename=dest)
    cake = fabio.open(dest)
    cakedata_list.append(cake.data)
    I, tth, chi = cake1
    print(I.shape)
    print(tth.shape)
    print(chi.shape)
    I_list.append(I)
    tth_list.append(tth)
    chi_list.append(chi)

cake_alldata = glob.glob(path + '/*_cake.edf')

cakedata_array = np.asarray(cakedata_list)
Idata_array = np.asarray(I_list)
tthdata_array = np.asarray(tth_list)
chidata_array = np.asarray(chi_list)

from pyFAI.gui import jupyter
fig, ax = subplots(1,  figsize=(10,8))

I_plot = I
tth_plot = tth
chi_plot = chi

cmap = plt.cm.inferno
```

```
levels = MaxNLocator(nbins=15).tick_values(0,I_plot.max()*.04)
norm = BoundaryNorm(levels, ncolors=cmap.N, clip=True)

ax.pcolormesh(tth_plot, chi_plot, I_plot, cmap=cmap, norm=norm)

ax.set_xlim(9.5,14.75)
ax.set_ylim(50,130)
ax.set_xlabel(r"2$\theta$ ($^{\circ}$)",
      fontsize = 24, color = 'k')
ax.set_ylabel(r"Azimuthal angle $\chi$ ($^{\circ}$)",
      fontsize = 24, color = 'k')
ax.set_title(r"2D XRD-measurement for $\mu = 7^{\circ}$",
      fontsize = 24, color = 'k')
fig.savefig('NewFinnishedSample2DScan30MinutesIn.png')

x = tth
b1 = np.where(13<x)
b2 = np.where(x<14)
B = np.intersect1d(b1,b2)

y = chi
d1 = np.where(80<y)
d2 = np.where(y<100)
D = np.intersect1d(d1,d2)

Total_intensity = 0
for k in B:
    Total_intensity = Total_intensity + np.sum(I[0:,k])
    #print(I[0:,k])

Sum_intensity = 0
for k in B:
    for i in D:
        Sum_intensity = Sum_intensity + I[i,k]
        #print(I[i,k])

print(Total_intensity)
print(Sum_intensity)
print(Sum_intensity/Total_intensity)
```

A.1 *In situ* sample

```
import time
import shutil, os
from silx.resources import ExternalResources
import pyFAI, fabio
import glob

t0 = time.perf_counter()
os.listdir()

notebook_path = os.path.abspath("Notebook.ipynb")
print(notebook_path)

path = os.path.abspath("[path to data folder]")
files = glob.glob(path + '/*.dat')
```

```
oldcake_alldata = glob.glob(path + '/*cake.dat')
for result in (oldcake_alldata):
    print("hi")
    print(result)
    os.remove(result)
    print("FileDeleted")
print(oldcake_alldata)

import numpy as np
i = -1

data_list = []

for dfile in files:
    i += 1
    data = np.loadtxt(dfile, dtype=float)
    data_list.append(data)
data_array = np.asarray(data_list)

import matplotlib.pyplot as plt
from matplotlib.colors import BoundaryNorm
from matplotlib.ticker import MaxNLocator
import numpy as np
import matplotlib as mpl
from matplotlib.pyplot import subplots

plt.rcParams['text.usetex'] = True

Ycoord_array = data_array[0, 0:, 0]
Xcoord_array = np.arange(0,720,1)
Xcoord_array = Xcoord_array
color_array = data_array[0:, 0:, 1]
plot_array = color_array.transpose()
plot_array = plot_array[:-1, :-1]

levels = MaxNLocator(nbins=15).tick_values(plot_array.min(), 0.3)
cmap = plt.cm.inferno
norm = BoundaryNorm(levels, ncolors=cmap.N, clip=True)

fig, ax = subplots(1, figsize=(15,5))

ax.pcolormesh(Xcoord_array, Ycoord_array, plot_array, cmap=cmap, norm=norm)
ax.set_title(r"In Situ Measurements of D170 NW array",
      fontsize = 24, color = 'k')
ax.set_xlabel(r"Frames (5s/frame)",
      fontsize = 24, color = 'k')
ax.set_ylabel(r"2$\theta$ ($^{\circ}$)",
      fontsize = 24, color = 'k')
ax.set_xlim(0,120)
xt = np.arange(0,120,5)
ax.set_xticks(xt)
fig.savefig('TimeResFig1.png')

all_images = glob.glob(path + '/*.tif')
ai = pyFAI.load("[path to calibration .poni file]")

cakedata_list = []
```

```
I_list = []
tth_list = []
chi_list = []

for one_image in all_images:
    fimg = fabio.open(one_image)
    dest = os.path.splitext(one_image)[0] + "_cake.edf"
    cake1 = ai.integrate2d_ng(fimg.data,
                    500, 360,
                    unit="2th_deg",
                    filename=dest)
    cake = fabio.open(dest)
    cakedata_list.append(cake.data)
    I, tth, chi = cake1
    I_list.append(I)
    tth_list.append(tth)
    chi_list.append(chi)

cake_alldata = glob.glob(path + '/*_cake.edf')

cakedata_array = np.asarray(cakedata_list)
Idata_array = np.asarray(I_list)
tthdata_array = np.asarray(tth_list)
chidata_array = np.asarray(chi_list)

from pyFAI.gui import jupyter

I_plot0 = Idata_array[12]
tth_plot0 = tthdata_array[12]
chi_plot0 = chidata_array[12]
steps = 1
for i in range(13, 24):
    I_plot0 = I_plot0 + Idata_array[i]
    steps += 1

I_plot1 = Idata_array[24]
tth_plot1 = tthdata_array[24]
chi_plot1 = chidata_array[24]
steps = 1
for i in range(25, 36):
    I_plot1 = I_plot1 + Idata_array[i]
    steps += 1

I_plot2 = Idata_array[36]
tth_plot2 = tthdata_array[36]
chi_plot2 = chidata_array[36]
steps = 1
for i in range(37, 48):
    I_plot2 = I_plot2 + Idata_array[i]
    steps += 1

I_plot3 = Idata_array[48]
tth_plot3 = tthdata_array[48]
chi_plot3 = chidata_array[48]
steps = 1
for i in range(49, 60):
    I_plot3 = I_plot3 + Idata_array[i]
    steps += 1
```

```
I_plot4 = Idata_array[60]
tth_plot4 = tthdata_array[60]
chi_plot4 = chidata_array[60]
steps = 1
for i in range(61, 72):
    I_plot4 = I_plot4 + Idata_array[i]
    steps += 1

I_plot5 = Idata_array[72]
tth_plot5 = tthdata_array[72]
chi_plot5 = chidata_array[72]
steps = 1
for i in range(73, 84):
    I_plot5 = I_plot5 + Idata_array[i]
    steps += 1

levels0 = MaxNLocator(nbins=15).tick_values(0,5)
print(I_plot0.min(),I_plot0.max())
norm0 = BoundaryNorm(levels0, ncolors=cmap.N, clip=True)

levels1 = MaxNLocator(nbins=15).tick_values(0,5)
print(I_plot1.min(),I_plot1.max())
norm1 = BoundaryNorm(levels1, ncolors=cmap.N, clip=True)


levels2 = MaxNLocator(nbins=15).tick_values(0,5)
print(I_plot2.min(),I_plot2.max())
norm2 = BoundaryNorm(levels2, ncolors=cmap.N, clip=True)


levels3 = MaxNLocator(nbins=15).tick_values(0,5)
print(I_plot3.min(),I_plot3.max())

norm3 = BoundaryNorm(levels3, ncolors=cmap.N, clip=True)


fig1 = plt.figure(figsize = (10,10))
plt.pcolormesh(tth_plot0, chi_plot0, I_plot0, cmap=cmap, norm=norm0)

plt.xlim(9,14.35)
plt.ylim(55,125)
plt.xlabel(r"2$\theta$ ($^{\circ}$)",
      fontsize = 24, color = 'k')
plt.ylabel(r"Azimuthal angle $\chi$ ($^{\circ}$)",
      fontsize = 24, color = 'k')
plt.title(r"2D XRD-measurement during frames 12-24",
      fontsize = 24, color = 'k')
plt.savefig('2DScan12-24.png')

fig2 = plt.figure(figsize = (10,10))
plt.pcolormesh(tth_plot1, chi_plot1, I_plot1, cmap=cmap, norm=norm1)

plt.xlim(9,14.35)
plt.ylim(55,125)
plt.xlabel(r"2$\theta$ ($^{\circ}$)",
      fontsize = 24, color = 'k')
plt.ylabel(r"Azimuthal angle $\chi$ ($^{\circ}$)",
```

```
      fontsize = 24, color = 'k')
plt.title(r"2D XRD-measurement during frames 24-36",
      fontsize = 24, color = 'k')
plt.savefig('2DScan24-36.png')

fig3 = plt.figure(figsize = (10,10))
plt.pcolormesh(tth_plot2, chi_plot2, I_plot2, cmap=cmap, norm=norm2)

plt.xlim(9,14.35)
plt.ylim(55,125)
plt.xlabel(r"2$\theta$ ($^{\circ}$)",
      fontsize = 24, color = 'k')
plt.ylabel(r"Azimuthal angle $\chi$ ($^{\circ}$)",
      fontsize = 24, color = 'k')
plt.title(r"2D XRD-measurement during frames 36-48",
      fontsize = 24, color = 'k')
plt.savefig('2DScan36-48.png')

fig4 = plt.figure(figsize = (10,10))
plt.pcolormesh(tth_plot3, chi_plot3, I_plot3, cmap=cmap, norm=norm3)
plt.xlim(9,14.35)
plt.ylim(55,125)
plt.xlabel(r"2$\theta$ ($^{\circ}$)",
      fontsize = 24, color = 'k')
plt.ylabel(r"Azimuthal angle $\chi$ ($^{\circ}$)",
      fontsize = 24, color = 'k')
plt.title(r"2D XRD-measurement during frames 48-60",
      fontsize = 24, color = 'k')
plt.savefig('2DScan48-60.png')

fig, ax = subplots(1, figsize=(10,8))
I_plot = Idata_array[360]
tth_plot = tthdata_array[360]
chi_plot = chidata_array[360]
steps = 1
for i in range(361, 420):
    I_plot = I_plot + Idata_array[i]
    steps += 1
print(steps)
levels = MaxNLocator(nbins=15).tick_values(0,0.25*I_plot0.max())
print(I_plot.min(),I_plot.max()*1)
norm = BoundaryNorm(levels, ncolors=cmap.N, clip=True)
ax.pcolormesh(tth_plot, chi_plot, I_plot, cmap=cmap, norm=norm)
ax.set_xlim(9.5,14.1)
ax.set_ylim(50,130)
ax.set_xlabel(r"2$\theta$ ($^{\circ}$)",
      fontsize = 24, color = 'k')
ax.set_ylabel(r"Azimuthal angle $\chi$ ($^{\circ}$)",
      fontsize = 24, color = 'k')
ax.set_title(r"2D XRD-measurement during frames 360-420",
      fontsize = 24, color = 'k')
fig.savefig('5MinLong2DScan30MinutesIn.png')

x = tth_plot
b1 = np.where(13<x)
b2 = np.where(x<14)
B = np.intersect1d(b1,b2)
```

```
y = chi_plot
d1 = np.where(80<y)
d2 = np.where(y<100)
D = np.intersect1d(d1,d2)

Total_intensity = 0
for k in B:
    Total_intensity = Total_intensity + np.sum(I_plot[0:,k])

Sum_intensity = 0
for k in B:
    for i in D:
        Sum_intensity = Sum_intensity + I_plot[i,k]
        #print(I[i,k])

print(Total_intensity)
print(Sum_intensity)
print(Sum_intensity/Total_intensity)

fig, ax = subplots(1, figsize=(15,5))
X1D=data_array[120,0:,0]
Y1D=data_array[120,0:,1]
steps = 1
for i in range(121, 132):
    Y1D = Y1D + data_array[i,0:,1]
    steps += 1
print(steps)
ax.plot(X1D,Y1D)
ax.set_title(r"In Situ XRD measurement: frames 120-136",
      fontsize = 20, color = 'k')
ax.set_xlabel(r"2$\theta$ ($^{\circ}$)",
      fontsize = 20, color = 'k')
ax.set_ylabel(r"Intensity (a.u.)",
      fontsize = 20, color = 'k')
ax.set_ylim(0,1.5)
fig.savefig('XRDPlot120-132.png')

x = data_array[120,0:,0]
a1 = np.where(9.6<x)
a2 = np.where(x<9.9)
A = np.intersect1d(a1,a2)
b1 = np.where(13<x)
b2 = np.where(x<15)
B = np.intersect1d(b1,b2)
C = np.concatenate((A,B))

for i in range(0, 720):
    print("New Scan",i)
    for k in C:
        sum_intensity = sum_intensity + data_array[i,k,1]

fig, ax = subplots(1, figsize=(15,5))
X1D_2 = np.arange(0,120,1)
Y1D_2 = []
Sum_2th=np.sum(X1D_2)
steps = 0
for i in range(0, 120):
    for k in C:
```

```
        sum_intensity = sum_intensity + data_array[i,k,1]
    Y1D_2.append(sum_intensity)
    sum_intensity = 0
    steps += 1

ax.plot(X1D_2,Y1D_2)
ax.set_xlim(0,120)
ax.set_ylim(6.75,8.125)
xticks=np.arange(0,120,5)
ax.set_xticks(xticks)
ax.set_xlabel(r"Frames (5s/frame)",
      fontsize = 24, color = 'k')
ax.set_ylabel(r"Intensity (a.u.)",
      fontsize = 24, color = 'k')
ax.set_title(r"In situ intensity over time",
      fontsize = 24, color = 'k')
fig.savefig('IntensityGrowth1.png')
fig, ax = subplots(1, figsize=(8,5))

X1D=data_array[12,0:,0]
Y1D=data_array[12,0:,1]
steps = 1
for i in range(13, 24):
    Y1D = Y1D + data_array[i,0:,1]
    steps += 1
print(steps)
ax.plot(X1D,Y1D)
ax.set_title(r"In Situ XRD measurement: frames 12-24",
      fontsize = 24, color = 'k')
ax.set_xlabel(r"2$\theta$ ($^{\circ}$)",
      fontsize = 24, color = 'k')
ax.set_ylabel(r"Intensity (a.u.)",
      fontsize = 24, color = 'k')
ax.set_ylim(0,2)
ax.set_xlim(9,14.5)
fig.savefig('EarlyXRDPlot1.png')

fig, ax = subplots(1, figsize=(8,5))
X1D=data_array[24,0:,0]
Y1D=data_array[24,0:,1]
steps = 1
for i in range(25, 36):
    Y1D = Y1D + data_array[i,0:,1]
    steps += 1
print(steps)
ax.plot(X1D,Y1D)
ax.set_title(r"In Situ XRD measurement: frames 24-36",
      fontsize = 24, color = 'k')
ax.set_xlabel(r"2$\theta$ ($^{\circ}$)",
      fontsize = 24, color = 'k')
ax.set_ylabel(r"Intensity (a.u.)",
      fontsize = 24, color = 'k')
ax.set_ylim(0,2)
ax.set_xlim(9,14.5)
fig.savefig('EarlyXRDPlot2.png')

fig, ax = subplots(1, figsize=(10,5))
X1D=data_array[36,0:,0]
```

```
Y1D=data_array[36,0:,1]
steps = 1
for i in range(37, 48):
    Y1D = Y1D + data_array[i,0:,1]
    steps += 1
print(steps)
ax.plot(X1D,Y1D)
ax.set_title(r"In Situ XRD measurement: frames 36-48",
      fontsize = 24, color = 'k')
ax.set_xlabel(r"2$\theta$ ($^{\circ}$)",
      fontsize = 24, color = 'k')
ax.set_ylabel(r"Intensity (a.u.)",
      fontsize = 24, color = 'k')
ax.set_ylim(0,2)
ax.set_xlim(8,15)
fig.savefig('EarlyXRDPlot3.png')

fig, ax = subplots(1, figsize=(15,5))
X1D=data_array[48,0:,0]
Y1D=data_array[48,0:,1]
steps = 1
for i in range(49, 60):
    Y1D = Y1D + data_array[i,0:,1]
    steps += 1
print(steps)
ax.plot(X1D,Y1D)
ax.set_title(r"In Situ XRD measurement: frames 48-60",
      fontsize = 24, color = 'k')
ax.set_xlabel(r"2$\theta$ ($^{\circ}$)",
      fontsize = 24, color = 'k')
ax.set_ylabel(r"Intensity (a.u.)",
      fontsize = 24, color = 'k')
ax.set_ylim(0,2.5)
fig.savefig('EarlyXRDPlot4.png')

fig, ax = subplots(1, figsize=(15,5))
X1D=data_array[0,0:,0]
Y1D=data_array[0,0:,1]
steps = 1
for i in range(1, 12):
    Y1D = Y1D + data_array[i,0:,1]
    steps += 1

print(steps)
ax.plot(X1D,Y1D)
ax.set_title(r"In Situ XRD measurement: frames 0-12",
      fontsize = 24, color = 'k')
ax.set_xlabel(r"2$\theta$ ($^{\circ}$)",
      fontsize = 24, color = 'k')
ax.set_ylabel(r"Intensity (a.u.)",
      fontsize = 24, color = 'k')
ax.set_ylim(0,2.5)
fig.savefig('EarlyXRDPlot4.png')
```